Global J. Environ. Sci. Manage. 9(1): 15-30, Winter 2023, Serial #33

Global Journal of Environmental Science and Management
(GJESM)

Homepage: https://www.gjesm.net/

ORIGINAL RESEARCH PAPER

Neural network-based classification of rock properties and seismic vulnerability

U. Muksin[1,*], E. Riana[1], A. Rudyanto[2], K. Bauer[3], A.V.H. Simanjuntak[2], M. Weber[3,4]

[1] *Tsunami and Disaster Mitigation Research Center, Universitas Syiah Kuala, Banda Aceh, Indonesia*

[2] *Meteorological, Climatological, and Geophysical Agency, Jakarta, Indonesia*

[3] *GFZ German Research Centre for Geosciences, Telegrafenberg, 14473 Potsdam, Germany*

[4] *University Potsdam, Karl-Liebknecht Street, 14476 Potsdam, Germany*

ARTICLE INFO

Article History:
Received 04 February 2022
Revised 21 May 2022
Accepted 26 June 2022

Keywords:
Earthquake
Neural network
Seismic vulnerability
Shear wave velocity
Soil and rock types

DOI: 10.22034/gjesm.2023.01.02

ABSTRACT

BACKGROUND AND OBJECTIVES: Soil or rock types in a region are often interpreted qualitatively by visually comparing various geophysical properties such as seismic wave velocity and vulnerability, as well as gravity data. Better insight and less human-dependent interpretation of soil types can be obtained from a joint analysis of separated and independent geophysical parameters. This paper discusses the application of a neural network approach to derive rock properties and seismic vulnerability from horizontal-to-vertical seismic ratio and seismic wave velocity data recorded in Majalengka-West Java, Indonesia.
METHODS: Seismic microtremors were recorded at 54 locations and additionally multichannel analyses of surface wave experiments were performed at 18 locations because the multichannel analyses of surface wave experiment needs more effort and space. From the two methods, the values of the average shear wave velocity for the upper 30 meters, peak amplitudes and the dominant frequency between the measurement points were obtained from the interpolation of those geophysical data. Neural network was then applied to adaptively cluster and map the geophysical parameters. Four learning model clusters were developed from the three input seismic parameters: shear wave velocity, peak amplitude, and dominant frequency.
FINDINGS: Generally, the values of the horizontal to vertical spectral ratios in the west of the study area were low (less than 5) compared with those in the southeastern part. The dominant frequency values in the west were mostly low at around 0.1–3 Hertz, associated with thick sedimentary layer. The pattern of the shear wave velocity map correlates with that of the horizontal to vertical spectral ratio map as the amplification is related to the soil or rock rigidity represented by the shear wave velocity. The combination of the geophysical data showed new features which is not found on the geological map such as in the eastern part of the study area.
CONCLUSION: The application of the neural network based clustering analysis to the geophysical data revealed four rock types which are difficult to observe visually. The four clusters classified based on the variation of the geophysical parameters show a good correlation to rock types obtained from previous geological surveys. The clustering classified safe and vulnerable regions although detailed investigation is still required for confirmation before further development. This study demonstrates that low-cost geophysical experiments combined with neural network-based clustering can provide additional information which is important for seismic hazard mitigation in densely populated areas

NUMBER OF REFERENCES	NUMBER OF FIGURES	NUMBER OF TABLES
42	6	0

*Corresponding Author:
Email: *muksin.umar@tdmrc.org*
Phone: +6281 2632 89103
ORCID: 0000-0001-7297-8065

Note: Discussion period for this manuscript open until April 1, 2023 on GJESM website at the “Show Article”.

INTRODUCTION

Site amplification, rock and soil properties and other subsurface characteristics are among key parameters in building construction (Day, 2012). Site amplification indicates how the ground motion in an area increases when seismic waves from an earthquake traverse. The shaking of sites due to earthquakes varies depending on the type of rocks and thickness of sediment layers. Horizontal shaking resulting from shear and surface waves is considered to contribute more to damage then vertical shaking. Therefore, the horizontal-to-vertical spectral ratio (HVSR) of seismic microtremors at natural resonance (dominant) frequency can be considered as site amplification. Nakamura (2009) showed a strong correlation between HVSR values and building damages. Building damage is also related to the natural frequency. When a seismic wave arrives at a site, a building shakes considerably if the dominant frequency of the ground motion of the site is close to the natural frequency of the building (Kham *et al*., 2006). The dominant frequency has also suggested to be related to the thickness of the subsurface structure underneath a site (Nakamura, 2009). When an earthquake occurs, physical properties (e.g., stiffness) of the soils of a site where a building is situated play crucial role in the level of building damage (Fat-Helbary *et al*., 2019). The stiffness of soil or rock can be represented by shear wave velocity. In general, the shear wave velocity increases with the stiffness of rock. Studies on the impact of earthquakes in Dinar, Turkey showed that an alluvial flat basin with a low Vs_{30} (average shear wave velocity over the upper 30-m soil profile) had the highest damage ratio (Kanlı *et al*., 2006). Engineers use Vs_{30} values to classify types of soil or rock in building standards (e.g., Ching and Winkel, 2018; Dobry *et al*., 2000). Rocks or soils with Vs_{30} within 180–360 meter per second (m/s) and 360–760 m/s are classified as stiff and very dense, respectively (BSSC, 1997). Soil with Vs_{30} less than 180 m/s are classified as soft and require a detailed investigation before buildings are constructed in a seismically active region. Shear wave velocity is also essential in the analysis of deterministic and probabilistic seismic hazards (Shreyasvi *et al*., 2019). For instance, the shear wave velocity at shallow depth is key input parameter in estimating ground motion. The Vs_{30} values of sites can be determined by multichannel surface-wave analysis (MASW) using active sources such as a sledgehammer (Park *et al*., 2007). Another approach to determining Vs_{30} is based on the inversion of microtremor data recorded by a single three-component seismometer (Arai and Tokimatsu, 2004). Alternatively, the less invasive spatial auto-correlation (SPAC) method can be used to determine the average shear wave velocity at a certain depth (Chávez-García *et al*., 2005). Hollender *et al*. (2018) applied modified spatial auto-correlation (MSPAC) using three component seismic records to determine the shear wave velocity structure. The SPAC and MSPAC methods need to have ambient noise sources to randomly distributed to obtain reliable velocity estimation (Hollender *et al*., 2018). Thus, MASW is more reliable in determining the seismic wave velocity. The determinations of shear wave velocity, predominant period, and seismic amplification are parts microzonation studies. Such microzonation studies are often conducted because the more accurate studies based on *in-situ* penetration test are much more expensive. A geological structure can be also studied using other geophysical methods, e.g., ambient noise tomography (Ryberg *et al*., 2016), traveltime body wave tomography (Muksin *et al*., 2013a) and attenuation tomography (Muksin *et al*., 2013b), and using seismic refraction and reflection imaging. Compared with the tomography method, HVSR and MASW analyses are low-cost and robust methods for investigating the near-surface geological structures of densely populated areas. Several authors have combined both Vs_{30} and HVSR data and qualitatively conducted a joint interpretation of soil or rock types and compared it with geology.

Asten *et al*. (2014) for example, suggested that the characteristics of Vs_{30} were strongly correlated with HVSR. Stanko and Markušić (2020) investigated an empirical relationship between Vs30 and HVSR (e.g., dominant frequency). The results showed that the relationship between the two parameters remains unclear with large standard deviation. There could be a relationship between Vs30 and H/V values because both parameters represent physical properties of rocks. In microzonation studies, the correlation between the shear wave velocity and HVSR parameters is commonly investigated by visually comparing the geophysical parameters (Gallipoli and Mucciarelli, 2009). An area is defined as less vulnerable if the region is characterized by high Vs30, low H/V and high dominant frequency. However, the wide ranges

of geophysical values make us difficult to derive the characteristics of rocks more precisely and objectively from visual interpretation. The development of neural network methods offers the possibility of improving the analysis of geophysical data and advancing the interpretation of various parameters objectively. One can interpret various rock types and site amplification using a less human-dependent method based on pattern recognition of collocated geophysical data. Clustering different types of data has become more frequently used in geospatial data analysis (Jena *et al*., 2020). For instance, the method of neural network has been used to correlate the shear wave velocity information with soil type microzonation based on the data pattern with visual interpretation (Nejad *et al*., 2018). Stambouli *et al.* (2017) applied a neural network approach to acceleration and HVSR data to infer characteristics of site amplification. The latter mentioned examples make use neural network methods with supervised learning, where desired output such as soil type are specified by the user as a kind of target function during training. Here we present an exemplary feasibility study for the usage of self-organizing maps (SOM) in regional seismic vulnerability evaluation based on HVSR and shear wave velocity data. The SOM approach is different from other neural network method by application of unsupervised learning. This can provide an alternative, unbiased view on vulnerability classification, as the clustering is not influenced by any presumptions in supervised neural network methods. Common geophysical site proxies are derived and analyzed by the SOM method. The resulting classification map is interpreted and discussed based on comparison with pre-existing geological mapping and petrophysical signatures of the derived clusters. Similar approaches have been applied by Bauer *et al.* (2020) where a combination of different seismic parameters from tomographic inversion was used to identify and map the distribution of different lithologies. The objective of the study is to investigate the correlation among the site amplification (H/V peak ratio), dominant frequency and Vs_{30} as well as to identify various geophysical signatures of soils or rocks from the data recorded in 2018 in Majalengka (West Java, Indonesia) by using the neural network method. The study area is a seismically active region surrounded by volcanic environment and highly populated city in West Java where earthquakes can occur along the subduction zone and several active faults around the area (Fig. 1). The microzonation study in the study area was conducted as the region is planned to be developed in the near future. The result of neural network analysis is compared with the results of previous geological survey to demonstrate the feasibility of the approach. This study has been carried out in Majalalengka, West Java in Indonesia in 2018.

Geology and tectonic setting of west Java and Majalengka

The tectonic setting of West Java illustrated in Fig. 1 is characterized by the northward movement of the Australian plate subducting beneath the Eurasian plate. The material subducted into the mantel is partially melted and rises to create several active volcanoes in west Java (Fig. 1). The combination of subduction, complicated plate motion, and crustal deformation triggers the presence of active faults in West Java including Cimandiri, Lembang, and Baribis (Fig. 1). These active faults and some volcanoes surround the district of Majalengka, which is populated by more than 1.1 million people, and hence earthquake risk in the region is high.

The closest active fault to Majalengka is the Baribis Fault (Fig. 1) extending from Subang to Majalengka (Supendi *et al.,* 2018). The Baribis Fault has recently generated earthquakes with magnitudes between Mw 2.0 and 4.7 (Pasari *et al*. 2020). The Baribis Fault is a thrust fault accommodating the relative motion between the Java and Sunda block (Koulali *et al.,* 2017). Daryono *et al.* (2019) suggested that the maximum magnitude of earthquakes on the Baribis Fault could reach Mw 6.5-7.0 based on the fault length; i.e., 29 kilometer (km), whereas the recurrence time of large earthquakes was estimated to be 170-670 years. Another fault close to Majalengka is the Lembang Fault (Fig. 1), which accommodates the trench parallel component of the Australian-Eurasian convergence. The recent activities of the Lembang Fault are indicated by an M 3.3 earthquake reported by Meteorological, Climatological, and Geophysical Agency (BMKG) of Indonesia in 2011, as also suggested by Afnimar and Rasmid (2015). Further southwest, the Lembang Fault is offset by an active Cimandiri thrust fault (Supendi *et al.,* 2018). Based on the fault length, the maximum magnitude of an earthquake that can occur along the Cimandiri Fault is approximately M 6.0–7.0 (Irsyam *et al.* 2017). Majalengka is surrounded

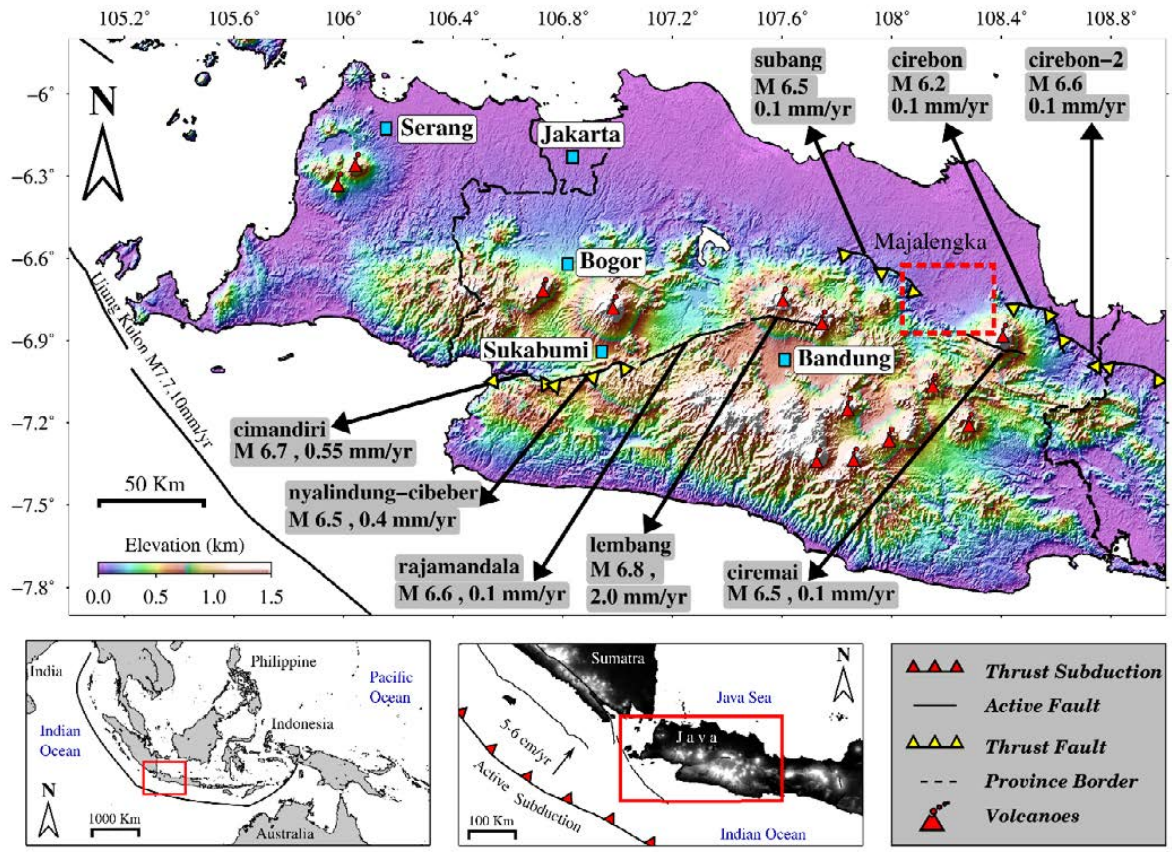

Fig. 1: (a) Geographical map of Indonesia and its surrounding with the study area (red square). (b) Seismicity map of West Java with the last decade's earthquake distribution; the volcano locations were obtained from Sparks *et al.* (2012). (c) The study area with the observation points of HVSR and MASW. The map is plotted using generic mapping tools (GMT) (Wessel *et al.* 2019); the fault lines were obtained from Irsyam *et al.* (2017).

by three main volcanoes: Tampomas in the west, Galunggung in the south, and Ciremai in the southeast of Majalengka as shown in Fig. 1. The Galunggung volcano erupted several times in 1822, 1894, 1918, and 1982–1983. Numerous fatalities were caused by the 1822 Galunggung eruption. The Ciremai stratovolcano was reported to erupt latest in 1937 without any fatality after the eruptions in 1772, 1775, and 1805 (Griffin, 2020). However, there is no report of the activity of the Tampomas volcano. The geology of Majalengka comprises tertiary sediments with intrusive and extrusive igneous rocks (Fig. 2). In the east, Majalengka generally comprises young volcanic products. The western part comprises Tjitjalang Formation and Aluvium. The Tjitjalang Formation consists of conglomerate, breccia, and sandstone. Further south, Majalengka comprises shale members and sandstone in the Tjinambo Formation (Fig. 2). As the region is surrounded by volcanoes, Majalengka is characterized by high topography with an elevation of 19–857 m above sea level. Thus, this hilly area is vulnerable to secondary impacts of seismic activities, such as landslides.

MATERIALS AND METHODS

Two geophysical experiments were performed to record 1) ambient seismic microtremor data and 2) controlled source MASW seismic data in Majalengka (West Java, Indonesia). The locations of the recording sites are marked with blue and red triangles in Fig.

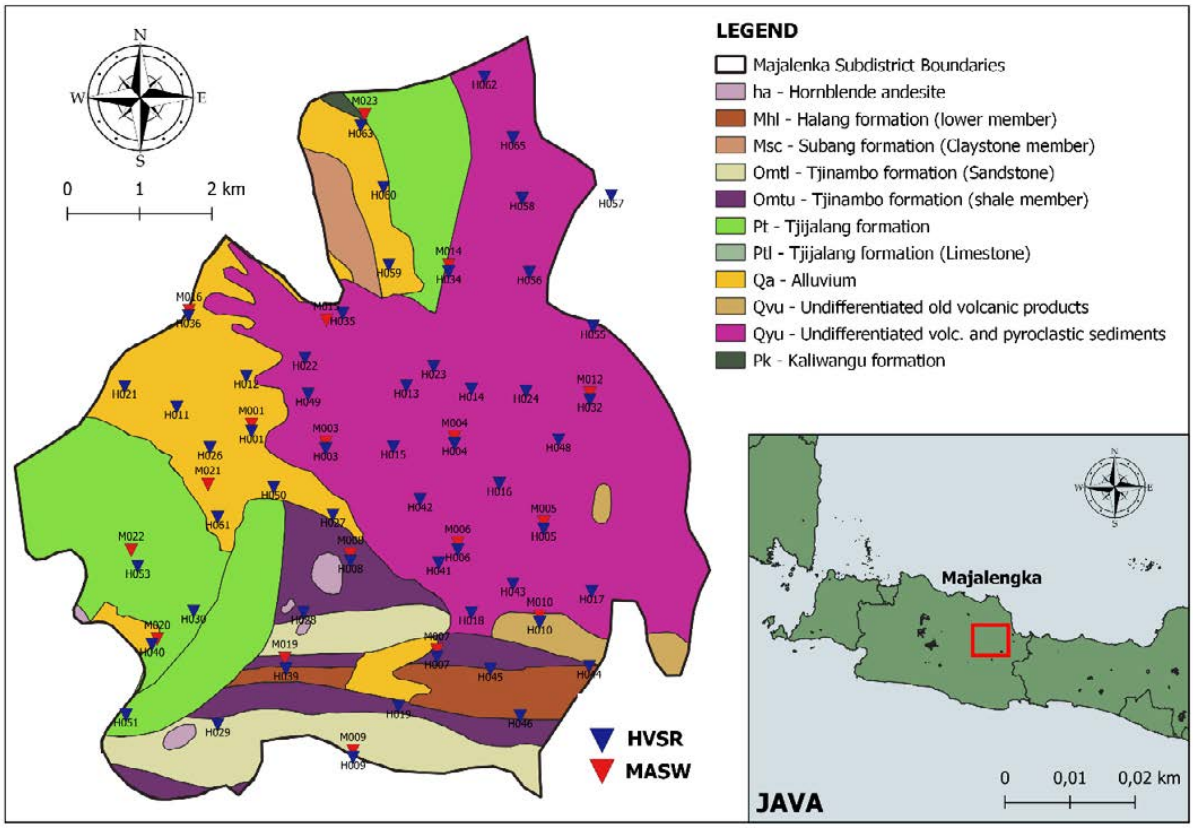

Fig. 2: Geology map of Majalengka (Modified from Djuri, 1995). The location of Majalengka on Java Island is shown in Fig. 1. The locations of the seismic experiments are indicated by red and blue triangles.

2. Particularly, the microtremor data were recorded at 54 sites indicated by blue triangles, whereas the MASW experiments, were performed at locations indicated by red triangles. Both deployments, seismic microtremor recordings and MASW experiments were relatively evenly distributed over the study area to interpolate and produce a representative map of the area.

HVSR data derived from seismic microtremor survey

The sources of seismic microtremors comprise the microseismic wave fields caused by human activities, the moon–earth interaction, and oceanic or tide-induced waves. The seismic microtremor measurements followed the procedure of SESAME (2004). A three-component short period seismometer, Lennartz Lite, equipped with a seismic data logger was deployed for 30 min to record seismic microtremors at each location. Then, the time-domain recording at each location was sub-divided into waveform segments of 50-s lengths. Waveform segments with transient noise, i.e., a sudden increase in the short-term-to-long-term average ratio, were excluded from the analysis. Thereafter, the fast Fourier transform was applied to the remaining 50-s waveform segments to transform the data from the time to frequency domain, and an algorithm from Konno and Ohmachi (1998) was applied for spectral smoothing. The horizontal and vertical components from all segments were stacked to obtain the averaged horizontal and vertical spectra for specific stations. After this stacking, HVSR was determined from the averaged spectra. The natural frequency (f_0) was determined at the

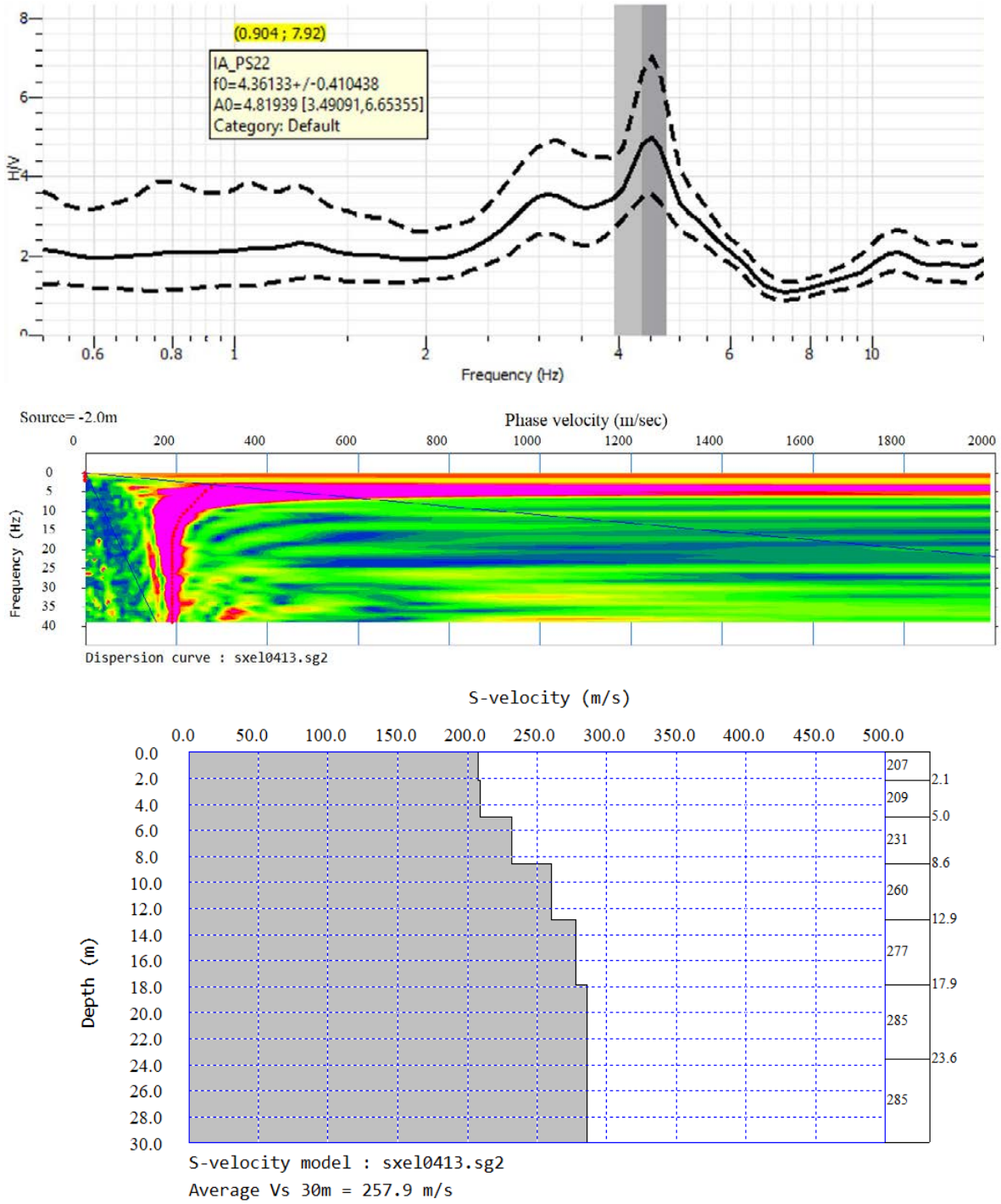

Fig. 3: HVSR of seismic microtremor at Point H020. The dominant frequency f_0 is the frequency when H/V is maximum (H/V) (TOP). Dispersion curve showing the relationship between phase velocity and frequency at location M040 (MIDDLE). Shear wave velocity model derived from the dispersion curve (BOTTOM).

highest HVSR peak. The site amplification is given by the squared HVSR peak at the natural frequency. An example of the HVSR curve at Point H020 is shown in Fig. 3. The analysis procedure of HVSR is presented in Nakamura (2000). Next, the HVSR and dominant frequency values were interpolated to obtain two-dimensional maps of the geophysical signatures of the study area.

Shear wave velocity modeling by using MASW

The data acquisition for the shear wave velocity investigation was performed using the MASW method in Majalengka, West Java, Indonesia (indicated by red triangles in Fig. 2). A 2 kg hammer was used as the seismic source, and seismic waves were recorded by a 2-m interval of 24 geophones. All geophones were connected to a seismic digitizer. The 2-m interval was chosen to be comparable to the minimum surface wavelength to avoid undesired spatial aliasing. The seismic lines were s*et al*ong a relatively flat 50 × 50-m^2 area to avoid significant changes in seismic recordings. The hammer was shot on the metal plate at one end of the seismic lines. The recordings were triggered by the hammer, and the seismic data were stored in the digitizer. The procedure of data acquisition for MASW followed the method described by Park *et al.* (1999). Then, the recordings from the forward and reverse shootings were transformed into a dispersion curve showing the relationship between the phase velocity of the Rayleigh wave and frequency (Fig. 3). Seismic surface waves with different wavelengths penetrate to different depths and propagate at different velocities. The dispersion curve is significantly influenced by S wave velocities for frequencies higher than 5 Hertz (Hz). Afterward, an iterative inversion method from Xia *et al.* (1999) was applied by imposing different S wave velocity models and layer thickness. Then, theoretical dispersion curves were calculated for different imposed models. The models (velocity and layer structure) were chosen as the final models when the theoretical and measured dispersion relation was closely fit. Examples of dispersion curves and resulting velocity models are shown in Fig. 3. As the inversion was applied for frequencies higher than 5 Hz, the consistently resolved depth range of the average velocity model was less than 30 m; hence, the velocity is called Vs_{30} (Xia *et al.*, 2002). The analysis was performed to obtain one-dimensional velocity models for all locations. The values of geophysical data, including Vs_{30}, HVSR, and dominant frequency between measurement points, were obtained from the data interpolation.

RESULTS AND DISCUSSION

An area is classified as a high level of seismic vulnerability if the H/V value is high and the dominant frequency is low (Nakamura, 2009), and the Vs30 value is low. An example for the seismic vulnerability analysis is shown for point H020 in Fig. 3. The bold line represents the HVSR result, whereas the dashed lines indicate the range of variations around the average curve. The maximum value of HVSR in the area of H020 is around 4.82. The dominant frequency (measured at the H/V peak) at Point H020 is 4.36 Hz which corresponds to a period of 0.23 s. The horizontal shaking due to an earthquake in the M005 area is suggested to be most amplified at frequencies of around 4.36 Hz. In general, the microtremor data are of good quality, so similar analyses could be performed for all 54 sites to determine the dominant frequency and H/V values. In addition, the MASW data are of good quality, supported by the fact that active sources and densely spaced multichannel receiver spreads were used in the experiments. Dispersion curves were determined (Fig. 3) and compared with theoretical curves to derive optimal 1D velocity models for each location.

The values of H/V peak, dominant frequency, and Vs_{30} for all locations were interpolated to plot the Majalengka map. The H/V peak ratios show variations between 1 and 7 (Fig. 4a), whereas the dominant frequencies vary between 0.2 and 12 Hz (Fig. 4b). At some points, the two geophysical data correlate. The highest amplification indicated by the H/V value is the Point H053 region (Fig. 2), which is also constituted by lower values of the dominant frequency. Fig. 4c shows the Vs_{30} map. The Vs_{30} values in Majalengka were between 234 and 606 m/s. The Vs_{30} map from Babakan to Majalengka (Fig. 4c) forms a pattern similar to the geology. Although Asten *et al* (2014) suggested a strong correlation between Vs30 and HVSR data, the comparison of the Vs30, H/V, dominant frequency values (Fig. 4) do not reveal clear correlation. Nevertheless, there was a clear anomaly in the east of the study area characterized by high H/V

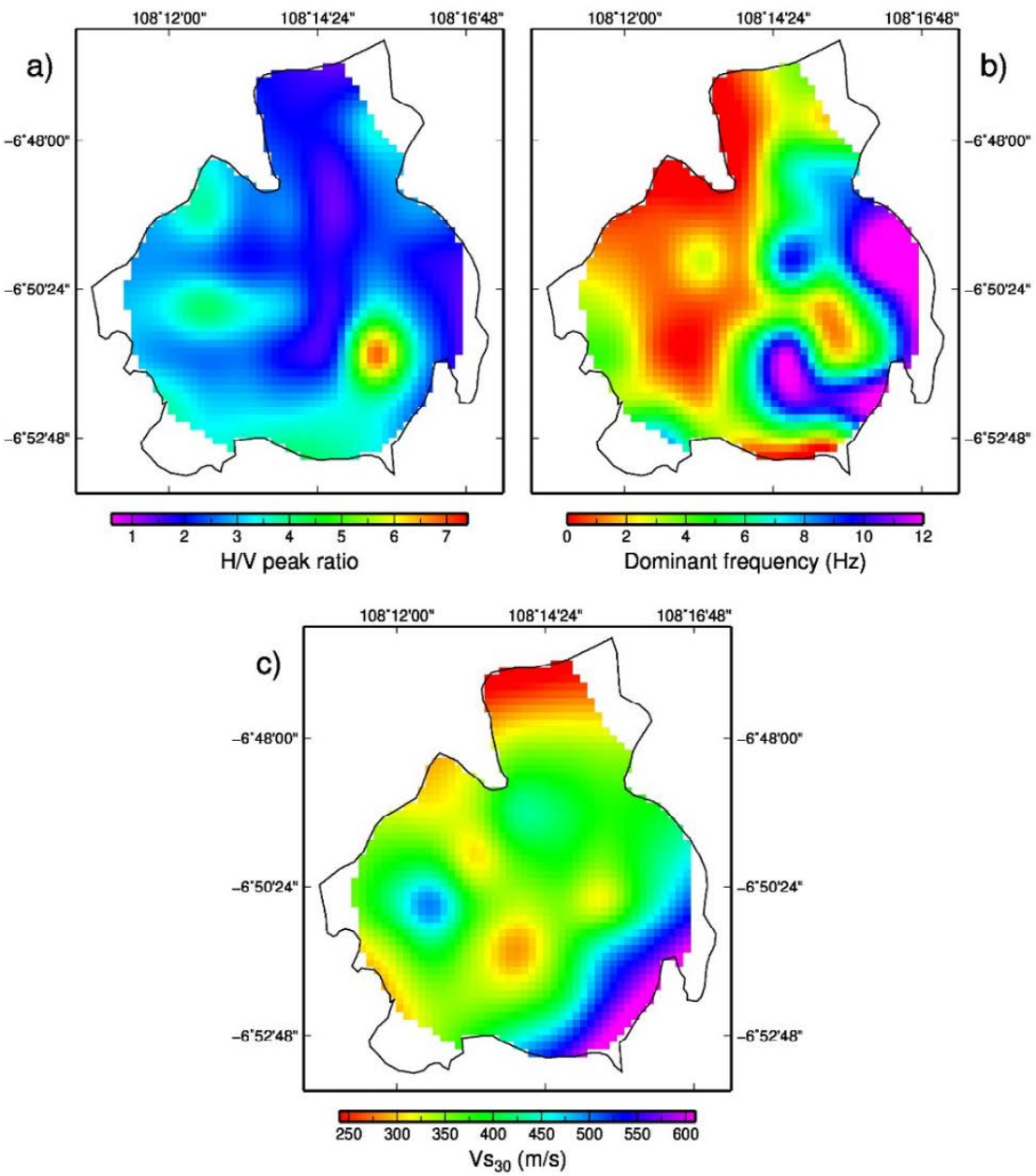

Fig. 4: Maps of interpolated seismic properties of (a) H/V peak ratio, (b) dominant frequency from ambient microtremor data, and (c) Vs_{30} derived from the MASW data. The black outline shows the district boundaries of Majalengka

value (between 6–7) and low dominant frequency (less than 2 Hz). There was also no clear empirical relationship between dominant frequency and Vs30 as suggested by Stanko and Markušić (2020). The three geophysical map is difficult to interpret based on visual comparison. Therefore, the correlation among the three geophysical parameters was analyzed by neural network clustering. Thereafter, the results were interpreted by additionally considering the geology.

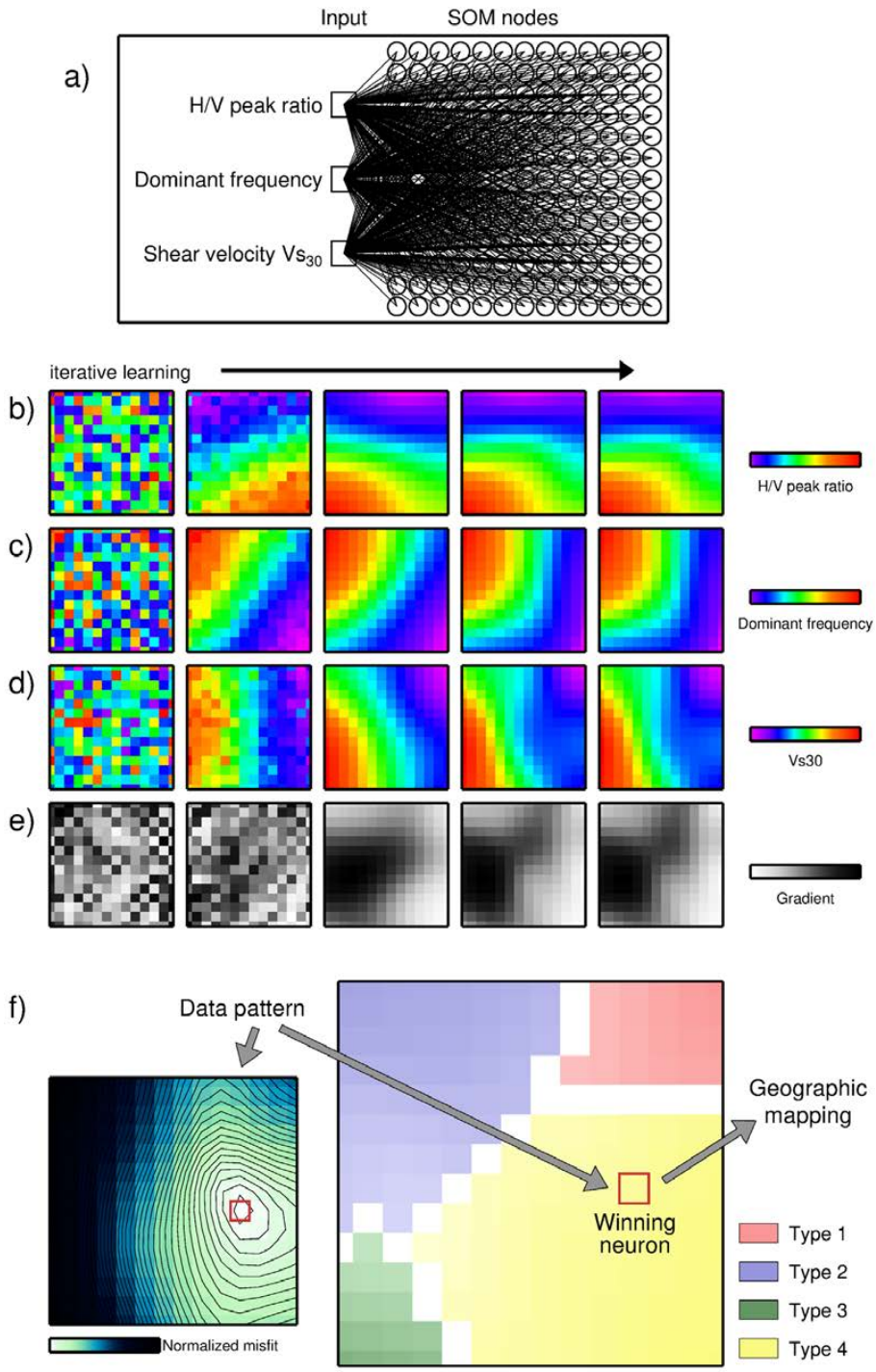

Fig. 5: (a) Design of the SOM which includes the input layer and a two-dimensional layout of SOM nodes. Evolution of the different components of the neural model vector (b-d) and the corresponding gradient function (e) during iterative learning. (f) Segmentation of the trained SOM. All input data patterns are classified based on the assignment of the winning neuron. The detection of the winning neuron is based on the evaluation of the normalized misfit function for a given data pattern vector. The associated color code is used in the geographic mapping of each input data pattern.

Neural Network clustering

The seismic parameters derived from the microtremor and MASW data (H/V peak ratio, dominant frequency, Vs_{30}) were combined and analyzed using a neural network clustering approach. The general objective was 1) to identify clusters with similar seismic properties which are related with well-defined rock properties and vulnerability and 2) to map the geographic distribution of the clusters. Kohonen (1990) introduced the concept of self-organizing maps (SOM) which is based on unsupervised learning and Bauer *et al.,* (2012) applied the method to geophysical data analyses. The SOM comprises an input layer and a two-dimensional arrangement of neurons (Kohonen, 1990). The input layer and neurons are fully connected (Fig. 5a). The values of H/V peak ratio, dominant frequency and Vs_{30} from the inversion at given surface points are converted into three-component input vectors. Equally, each SOM neuron is represented by a three-component neural model vector. Before learning, the values of all neural model vector components are initialized with random numbers. During iterative learning, input vectors are randomly chosen and a learning rule is applied (Bauer *et al.,* 2008). The so-called winning neurons with model vectors most similar to the input vector are modified to improve similarity between the input vector and the winning neural model vector. Such modification is also applied to the neighboring neurons of the winning neuron, but to a smaller degree. The effects of the iterative learning are illustrated in Fig. 5b–d. The model vector components show a random distribution over the SOM at the first iteration (left panels in Fig. 5b–d). With increasing iterations during learning, a systematic distribution develops across the SOM (right panels in Fig. 5b–d). Consequently, similar input vectors are associated with winning neurons at specific regions at the SOM. These specific clustering regions show small variations in the neural model vector components of neighboring neurons due to the learning rule. We use a gradient function to detect these regions based on small gradient values (Bauer *et al.*, 2012). The separation of different clustering regions is indicated by large gradient values (dark colors in Fig. 5e). The gradient function is finally used for an automated definition of clusters in the trained SOM using an image processing technique called watershed segmentation (Bauer *et al.*, 2020). In this procedure, we firstly identify regions with low gradient (Fig. 5e). For each of those regions, the surrounding ridge with high gradient (watershed) is determined and used to define the outer boundary of the cluster at the SOM. The different clustering regions are color-coded where the gradient function is used to modify the color intensity (Fig. 5f). More insight into the application of the watershed segmentation algorithm is presented by example in Bauer *et al.* (2012). The gradient function is finally used for SOM automated segmentation (Bauer *et al.,* 2020). The different clustering regions are color-coded, where the gradient function is used to modify the color intensity (Fig. 5f). Ultimately, for each winning neural vector, the related rock type with the corresponding color is used for plotting the geographical map.

Joint analysis and interpretation

The result of the neural network analysis is a clustering of the data into groups with similar petrophysical properties (classification). The classification was based on the values of Vs30, H/V value and dominant frequency as shown in Fig. 6. The geological interpretation is based on (1) comparison of the geographic distribution with pre-existing maps, and (2) by consideration of the petrophysical signature of each cluster. The Neural Network clustering provided four types of near-surface rocks (Types 1–4) and vulnerability in Majalengka (Fig. 5f). The geographic distribution of Types 1–4 is shown in Fig. 6a. Each type is related to well-defined values of H/V peak ratio (Fig. 6b), dominant frequency (Fig. 6c), and Vs_{30} (Fig. 6d). The rocks classified as Type 1 (red colors in Fig. 6) are characterized by low amplification with H/V peak ratios of around 2, low dominant frequencies (below 5 Hz), and low Vs_{30} velocities (between 200 and 380 m/s). The Type 1 rocks comprise Alluvium and claystone with limestone beds of the Subang Formation (the geology of Majalengka in Fig. 2) and are mainly located in the northern part and some parts in the center of Majalengka. The Subang Formation and Alluvium are considered as stiff soils, which are consistent with Vs_{30} velocities between 200 and 350 m/s. However, the HVSR and dominant frequency values of the areas comprising Type 1 rocks are low. A low dominant frequency is normally associated with a thick layer of rocks or sediments; therefore, the vulnerability is high. The Type 2 rocks (blue colors in Fig. 6) are characterized by moderate Vs_{30}, low HVSR, and high dominant frequency values.

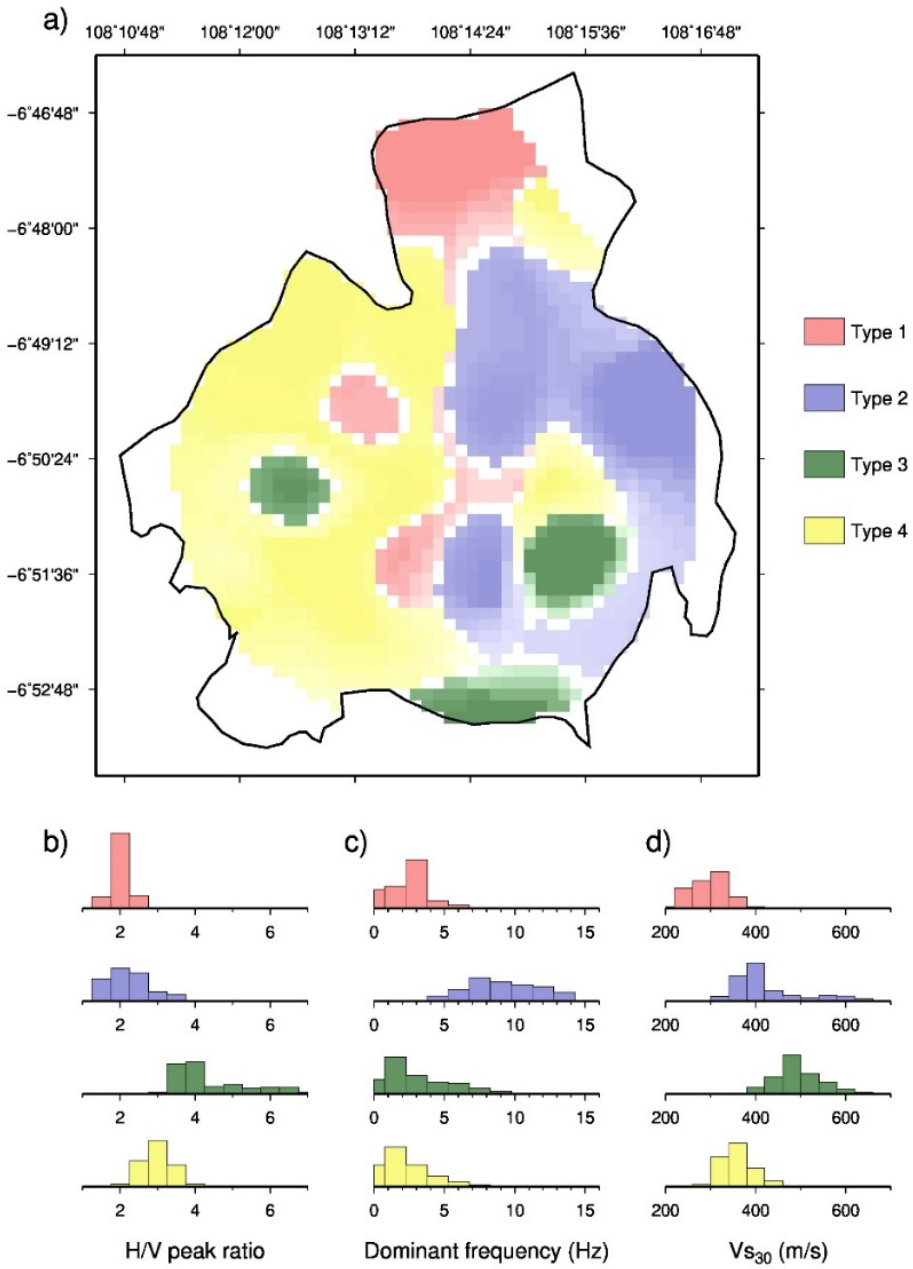

Fig. 6: (a) Geographic distribution of four types of near-surface rocks and vulnerability based on neural network clustering of petrophysical properties in Majalengka. Histograms of (a) H/V peak ratio, (b) dominant frequency, and (c) Vs_{30} for Types 1–4.

The Type 2 rocks are situated mostly on the east side of Majalengka and comprise young volcanic products, e.g., andesitic and basaltic lava from the Tampomas and Ceremai volcanoes (Marliyani *et al.,* 2020). The geology of the Type 2 rocks agrees with their geophysical properties. The seismic wave propagates faster within the volcanic rocks than within sedimentary rocks. Areas comprising dense rock are characterized by low amplification and high values of dominant frequency (Leyton *et al.,* 2013).

The geophysical and geological data reveal that sites within the cluster of Type 2 rocks are the safest areas from earthquake damage.

If we look at the geographic distribution of the Type 3 rocks (green colors in Fig. 6) and compare with the geological map from Djuri (1995), the type 3 cluster is associated with the Cinambo Formation, comprising sandstone and graywacke members. The cluster's areas comprise very dense soil or soft rock as indicated by high Vs_{30} values above 400 m/s. Moreover, moderate-to-high amplification is indicated by the high H/V peak ratios of above 3, whereas the dominant frequencies are low. This combination of high H/V peak ratios and low dominant frequencies can be explained by a thick subsurface layer of the Cinambo Formation. Djuri (1995) estimated the thickness of the Cinambo Formation to be between 400 and 500 m. A tall building located on a low dominant frequency site, such as the thick Cinambo Formation is highly vulnerable as it responds sensitively to low frequency shaking. The Type 4 rocks (yellow colors in Fig. 6) cover the largest area and occur mainly in the western part of Majalengka. Comparison with the geological map indicates that Type 4 is associated with the Citalang Formation, comprising tuffaceous sandstone and conglomerate (Zaputlyaeva *et al.,* 2020). The histograms in Figs. 6b–d show moderate amplification (H/V peak ratios of 2–4), low dominant frequencies, and moderate Vs_{30} values (300–450 m/s) for this rock type. Based on this petrophysical and lithological characterization, the areas classified as Type 4 are relatively safe from seismic shaking and hence suitable for future development.

CONCLUSION

Three key geophysical parameters, Vs_{30}, H/V, and dominant frequency, were mapped in Majalengka based on a micro-zonation study. The eastern part of Majalengka is considered more vulnerable as H/V value is higher and the dominant frequency is lower than those in the western part. The Vs_{30} values are generally between 220 and 400 m/s, except in a particular area in the east that is visually similar to the dominant frequency pattern. The pattern of Vs_{30} correlates relatively well with the geology in a certain zone of the study area. Several possible geological features represented by the geophysical anomalies from the H/V, dominant frequency, and Vs_{30} data not found in the geological map are revealed. Visual observation shows that the western part of Majalengka is more vulnerable than the eastern part. Although the patterns of the three geophysical maps resulting from the conventional data analysis seem to relate to each other, it is difficult to classify different types of rocks and vulnerability in detail from visual observation. As an alternative approach for such vulnerability evaluation, the SOM method, an unsupervised NN-based approach, was applied to the three combined geophysical parameters in the form of data pattern vectors. The NN-based SOM method successfully defined four clusters associated with different rock types and related degrees of vulnerability in Majalengka derived from the three geophysical parameters. Each cluster correspond to a set of data pattern vectors representing similar underlying geophysical properties.

The characteristics of the clusters correlate well with pre-existing geological information, showing that the two largest clusters are those for the Type 2 rocks, in the east, comprising young volcanic products, such as andesitic and basaltic lava, and the Type 4 rocks, in the west, comprising tuffaceous sandstone and conglomerate. These two largest clusters are considered safe for future development because the areas are characterized by moderate-to-high Vs_{30} values and low seismic amplification. Two smaller clusters comprising Types 1 and 3 rocks require more detailed studies before future developments are undertaken. These two smaller areas are characterized by low Vs_{30} values of Alluvium (Type 1) and thick layers of sandstone with high amplification and low dominant frequency (Type 3). The application of the NN-based SOM method revealed several safe zones located within seismically vulnerable areas, e.g., Type 3 rocks located within Type 4 rocks in the western and eastern part of Majalengka, which are difficult to be distinguished by visual observation and comparison of the three geophysical maps. Another advantage of the NN-based SOM application is that a small cluster of rocks can be automatically identified inside a larger cluster as the Type 3 is situated inside the Type 4. Future research could include comparison with similar multiparameter interpretation approaches and additional involvement of vulnerability modeling.

AUTHOR CONTRIBUTIONS

U. Muksin, the corresponding author, has contributed in supervising the second author in the data analysis HVSR and MASW, interpreted the results, and preparing the manuscript. E. Riana performed HVSR and MASW data analysis. A. Rudiyanto designed the field experiment and conducted field data acquisition as well as contributed in the HVSR and MASW data analysis. A.V.H. Simanjuntak prepared all the maps and figures and interpretation of the results. K. Bauer implemented and applied the neural network analysis and prepared related text and figures. M. Weber participated in the interpretation of the SOM results and manuscript preparation.

ACKNOWLEDGEMENT

The experiment was conducted in Majalengka, West Java Indonesia by the team from Meteorological, Climatological, and Geophysical Agency of Indonesia (BMKG). The data analysis and preparation of the manuscript was a part of the World Class Professor (WCP) funded by the Ministry of Education, Culture, Research and Technology of Indonesia with the Contract Number: [T46/D2.3/KK.04.05/2019]. The proofreading of the manuscript is supported by SupeRISKa research project with the Contract Number [PRJ-103/LPDP/2021].

CONFLICT OF INTEREST

The author declares that there is no conflict of interests regarding the publication of this manuscript. In addition, the ethical issues, including plagiarism, informed consent, misconduct, data fabrication and/or falsification, double publication and/or submission, and redundancy have been completely observed by the authors.

ABBREVIATIONS

1D	1 – Dimension
2D	2 – Dimension
3D	3-component
BMKG	Badan Meteorologi Klimatologi dan Geofisika (Meterological, Climatological and Geophysical Agency of Indonesia)
cm/y	Centimeter per year
e.g	Exempli gratia (for example)
f_0	Dominant frequency
GMT	Generic mapping tools
H020	HVSR observation point number 20
H053	HVSR observation point number 53
Ha	Hornblende andesite
HVSR	Horizontal to vertical spectral ratio
H/V	Horizontal over vertical
Hz	Hertz
i.e.	Id est (that is)
kg	Kilogram
km	Kilometer
LTA	Long-Term Average
m	Meter
M	Magnitude
MASW	Pearson correlation coefficient
Mhl	Halang formation (lower member)

Msc	Subang formation
Mw	Magnitude moment
m/s	Meter per second (velocity unit)
m^2	Meter square
mm/y	Millimeter per year
M005	MASW observation point number 05
M024	MASW observation point number 24
NN	Neural Network
Pk	Kaliwangu formation
Pt	Tjijalang formation
Ptl	Tjijalang formation with limestone
Qa	Alluvium formation
Qmtl	Tjinambo formation with sandstone
Qmtu	Tjinambo formation with shale
Qvu	Undifferentiated old volcanic products
Qyu	Undifferentiated volcanic and pyroclastic sediments
s	Second
SPAC	Spatial auto-correlation
MSPAC	Modified spatial auto-correlation
STA	Short-term average
S wave	Shear wave
SOM	Self-organizing maps
Type 1	First type of neural network results
Type 2	Second type of neural network results
Type 3	Third type of neural network results
Type 4	Fourth type of neural network results
Vs	Shear wave velocity
Vs_{30}	Shear wave velocity at depth of 30 m

REFERENCES

Afnimar, A.; Rasmid, R., (2015). Geological and tectonic implications obtained from first seismic activity investigation around Lembang fault. Geosci. Lett., 2(1): 1-11 **(11 pages).**

Jena, R.; Pradhan, B.; Beydoun, G., (2020). Earthquake vulnerability assessment in Northern Sumatra province by using a multi-criteria decision-making model. International journal of disaster risk reduction, 46(2020): 101518 (**14 pages)**.

Arai, H.; Tokimatsu, K., (2004). S-wave velocity profiling by inversion of microtremor H/V spectrum. Bull. Seismol. Soc. Am., 94(1): 53-63 **(11 pages).**

Fat-Helbary, R.E.S., El-Faragawy, K.O.; Hamed, A., (2019). Application of HVSR technique in the site effects estimation at the south of Marsa Alam city, Egypt. J. Afr. Earth. Sci., 154(2019): 89-100 (**12 pages)**.

Asten, M.W.; Askan, A.; Ekincioglu, E.E.; Sisman, F.N.; Ugurhan, B., (2014). Site characterisation in north-western Turkey based on SPAC and HVSR analysis of microtremor noise. Explor. Geophys., 45(2): 74-85 **(12 pages).**

Bauer, K.; Muñoz, G.; Moeck, I., (2012). Pattern recognition and lithological interpretation of collocated seismic and magnetotelluric models using self-organizing maps. Geophys. J. Int., 189 (2): 984-998 (**16 pages**).

Bauer, K.; Norden, B.; Ivanova, A.; Stiller, M.; Krawczyk, C.M., (2020). Wavelet transform-based seismic facies classification and modelling: application to a geothermal target horizon in the NE German Basin. Geophys. Prospec., 68(2): 466-482 **(17 pages).**

Bauer, K.; Pratt, R.; Haberland, C.; Weber, M., (2008). Neural network analysis of crosshole tomographic images: The seismic signature of gas hydrate bearing sediments in the Mackenzie Delta (NW Canada), Geophys. Res. Lett., 35(19): 1 - 6 **(6 pages**).

BSSC, (1997). NEHRP recommended provisions for seismic regulations for new buildings and other structures. Building Seismic Safety Council, FEMA, 302: 303.

Chávez-García, F.J.; Rodríguez, M.; Stephenson, W.R.; (2005). An alternative approach to the SPAC analysis of microtremors: exploiting stationarity of noise. Bull. Seismol. Soc. Am., 95(1): 277-293 **(17 pages).**

Ching, F.D.; Winkel, S.R., (2018). Building Codes Illustrated: A Guide to Understanding the 2018 International Building Code. edn, Vol., John Wiley & Sons.

Daryono, M.R.; Natawidjaja, D.H.; Sapiie, B.; Cummins, P., (2019). Earthquake geology of the lembang fault, West Java, Indonesia. Tectonophysics. 751(2019): 180-191 **(12 pages).**

Day, R.W., (2012). Geotechnical Earthquake Engineering Handbook: With the 2012 International Building Code. McGraw-Hill Professional.

Djuri, M., (1995). Peta Geologi lembar Arjawinangun, Jawa, skala 1: 100.000. Puslitbang Geologi, Bandung.

Dobry, R.; Borcherdt, R.; Crouse, C.; Idriss, I.; Joyner, W.; Martin, G.R.; Power, M.; Rinne, E.; Seed, R., (2000). New site coefficients and site classification system used in recent building seismic code provisions. Earthquake Spectra, 16(1): 41-67 **(27 pages).**

Gallipoli, M.R.; Mucciarelli, M., (2009). Comparison of site classification from VS 30, VS 10, and HVSR in Italy. Bull. Seismol. Soc. Am., 99(1): 340-351 **(12 pages).**

Griffin, C., (2020). Prosperity beyond belief: The interaction between a potato crop boom, vulnerability and volcanic hazard in Central Java, Indonesia. Singapore J. Trop. Geogr., 41(1): 23-39 **(17 pages).**

Hollender, F.; Cornou, C.; Dechamp, A.; Oghalaei, K.; Renalier, F.;

Maufroy, E.; Burnouf, C.; Thomassin, S.; Wathelet, M.; Bard, P.-Y., (2018). Characterization of site conditions (soil class, V S30, velocity profiles) for 33 stations from the French permanent accelerometric network (RAP) using surface-wave methods. Bull. Earthquake Eng., 16(6): 2337-2365 **(29 pages).**

Irsyam, M.; Widiyantoro, S.; Natawidjaja, D.; Meilano, I.; Rudyanto, A.; Hidayati, S.; Triyoso, W.; Hanifa, N.; Djarwadi, D.; Faizal, L., (2017). Peta Sumber and Bahaya Gempa Indonesia tahun 2017, Pusat Penelitian and Pengembangan Perumahan dan Permukiman, Badan Penelitian and Pengembangan, Kementerian Pekerjaan Umum and Perumahan Rakyat.

Kanlı, A.I.; Tildy, P.; Prónay, Z., Pınar, A.; Hermann, L., (2006). VS 30 mapping and soil classification for seismic site effect evaluation in Dinar region, SW Turkey. Geophys. J. Int., 165(1): 223-235 **(13 pages).**

Kham, M.; Semblat, J.-F.; Bard, P.-Y.; Dangla, P., (2006). Seismic site–city interaction: main governing phenomena through simplified numerical models. Bull. Seismol. Soc. Am., 96(5): 1934-1951 **(28 pages).**

Kohonen, T., (1990). The self-organizing map. Proc. IEEE, 78(9): 1464-1480 (**17 pages).**

Konno, K.; Ohmachi, T., (1998). Ground-motion characteristics estimated from spectral ratio between horizontal and vertical components of microtremor. Bull. Seismol. Soc. Am., 88(1): 228-241 **(14 pages).**

Koulali, A.; McClusky, S.; Susilo, S.; Leonard, Y.; Cummins, P.; Tregoning, P.; Meilano, I.; Efendi, J.; Wijanarto, A., (2017). The kinematics of crustal deformation in Java from GPS observations: Implications for fault slip partitioning. Earth Planet. Sci. Lett., 458(2017): 69-79 (**11 pages).**

Leyton, F.; Ruiz, S.; Sepúlveda, S.; Contreras, J.; Rebolledo, S.; Astroza, M., (2013). Microtremors' HVSR and its correlation with surface geology and damage observed after the 2010 Maule earthquake (Mw 8.8) at Talca and Curicó, Central Chile. Eng. Geol., 161(2013): 26-33 **(8 pages).**

Marliyani, G.I.; Helmi, H.; Arrowsmith, J.R.; Clarke, A., (2020). Volcano morphology as an indicator of stress orientation in the Java Volcanic Arc. Indonesia. J. Volcanol. Geotherm. Res., 400: 106912 (**19 pages).**

Muksin, U.; Bauer, K.; Haberland, C., (2013a). Seismic Vp and Vp/Vs structure of the geothermal area around Tarutung (North Sumatra, Indonesia) derived from local earthquake tomography. J. Volcanol. Geotherm. Res., 260(2013): 27-42 **(16 pages).**

Muksin, U.; Haberland, C.; Bauer, K.; Weber, M., (2013b). Three-dimensional upper crustal structure of the geothermal system in Tarutung (North Sumatra, Indonesia) revealed by seismic attenuation tomography. Geophys. J. Int., 195(3): 2037-2049 **(13 pages).**

Nakamura, Y., (2000). Clear identification of fundamental idea of Nakamura's technique and its applications. in Proceedings of the 12th world conference on earthquake engineering Auckland New Zealand.

Nakamura, Y., (2009). Basic structure of QTS (HVSR) and examples of applications, Increasing Seismic Safety by Combining Engineering Technologies and Seismological Data. 33-51 **(19 pages).**

Nejad, M.M.; Momeni, M.S.; Manahiloh, K.N., (2018). Shear wave velocity and soil type microzonation using neural networks and geographic information system. Soil Dyn. Earthquake Eng., 104(2018): 54-63 (**10 pages**).

Pasari, S.; Simanjuntak, A.V.; Mehta, A.; Sharma, Y., (2021). The Current State of Earthquake Potential on Java Island, Indonesia. Pure Appl. Geophys., 178(8): 2789-2806 (**18 pages**).

Park, C.B.; Miller, R.D.; Xia, J., (1999). Multichannel analysis of surface waves. Geophysics. 64(3): 800-808 (**9 pages**).

Park, C.B.; Miller, R.D.; Xia, J.; Ivanov, J., (2007). Multichannel analysis of surface waves (MASW)—active and passive methods. The Leading Edge. 26(1) 60-64 (**5 pages**).

Ryberg, T.; Muksin, U.; Bauer, K., (2016). Ambient seismic noise tomography reveals a hidden caldera and its relation to the Tarutung pull-apart basin at the Sumatran Fault Zone, Indonesia. J. Volcanol. Geotherm. Res., 321(2016): 73-84 (**12 pages**).

SESAME, W., (2004). Guidelines for the implementation of the H/V spectral ratio technique on ambient vibrations-Measurements, processing and interpretation. SESAME European research project, Deliverable D23. 12., Project No, European Commission—Research General Directorate **(62 pages)**.

Selles, A.; Deffontaines, B.; Hendrayana, H.; Violette, S., (2015). The eastern flank of the Merapi volcano (Central Java, Indonesia): Architecture and implications of volcaniclastic deposits. J. Asian Earth Sci., 108(2015): 33-47 (**15 pages**).

Shreyasvi, C.; Venkataramana, K.; Chopra, S., (2019). Local site effect incorporation in probabilistic seismic hazard analysis–A case study from southern peninsular India, an intraplate region. Soil Dyn. Earthquake Eng., 123(2019): 381-398 (**18 pages**).

Sparks, R.S.J.; Biggs, J.; Neuberg, J.W., (2012). Monitoring volcanoes. Science, 335(6074), 1310-1311 (**2 pages**).

Stambouli, A.B.; Zendagui, D.; Bard, P.-Y.; Derras, B., (2017). Deriving amplification factors from simple site parameters using generalized regression neural networks: implications for relevant site proxies. Earth Planets Space. 69(1): 99-115 (**27 pages**).

Stanko, D.; Markušić, S., (2020). An empirical relationship between resonance frequency, bedrock depth and VS30 for Croatia based on HVSR forward modelling. Nat. Hazard., 103(3): 3715-3743 (**29 pages**).

Supendi, P.; Nugraha, A.D.; Puspito, N.T.; Widiyantoro, S.; Daryono, D., (2018). Identification of active faults in West Java, Indonesia, based on earthquake hypocenter determination, relocation, and focal mechanism analysis. Geosci. Lett., 5(1): 1-10 (**10 pages**).

Wessel, P.; Luis, J. F.; Uieda, L.; Scharroo, R.; Wobbe, F.; Smith, W. H.; Tian, D. (2019). The generic mapping tools version 6. Geochem. Geophys. Geosyst., 20(11): 5556 - 5564 (**252 pages**).

Xia, J.; Miller, R.D.; Park, C.B., (1999). Estimation of near-surface shear-wave velocity by inversion of Rayleigh waves. Geophysics. 64(3): 691-700 (**10 pages**).

Xia, J.; Miller, R.D.; Park, C.B.; Hunter, J.A.; Harris, J.B.; Ivanov, J., (2002). Comparing shear-wave velocity profiles inverted from multichannel surface wave with borehole measurements. Soil Dyn. Earthquake Eng., 22(3): 181-190 (**10 pages**).

Zaputlyaeva, A.; Mazzini, A.; Blumenberg, M.; Scheeder, G.; Kürschner, W.M.; Kus, J.; M.T., Jones.; Frieling, J., (2020). Recent magmatism drives hydrocarbon generation in north-east Java, Indonesia. Sci. Rep., 10(1): 1-14 (**14 pages**).

AUTHOR (S) BIOSKETCHES

Muksin, U., Ph.D., Associate Professor, Tsunami and Disaster Mitigation Research Center, Universitas Syiah Kuala, Jl. Professor Dr. Ibrahim Hasan, Gampong Pie, Indonesia.
- Email: *muksin.umar@tdmrc.org*
- ORCID: 0000-0001-7297-8065
- Web of Science ResearcherID: W-3934-2018
- Scopus Author ID: 55795600300
- Homepage: http://fsd.unsyiah.ac.id/muksinumar/

Ennita, R., B.Sc. Master Student, Bandung Institute of Technology (ITB), Jl. Ganesa No.10, Lb. Siliwangi, Kota Bandung, Jawa Barat, Indonesia.
- Email: *ennitariana12@gmail.com*
- ORCID: 0000-0002-7517-0982
- Web of Science ResearcherID: NA
- Scopus Author ID: NA
- Homepage: http://tdmrc.unsyiah.ac.id/

Rudyanto, A., M.Phil. Head of Engineering Seismology. Meteorological, Climatological, and Geophysical Agency of Indonesia (BMKG), Kemayoran, Jakarta, Indonesia.
- Email: *ariska.rudyanto@bmkg.go.id*
- ORCID: 0000-0002-8774-9449
- Web of Science ResearcherID: NA
- Scopus Author ID: 56943549200
- Homepage: http://www.bmkg.go.id/

Simanjuntak, A.V.H., Ph.D. Candidate, Tsunami and Disaster Mitigation Research Center, Universitas Syiah Kuala, Jl. Professor Dr. Ibrahim Hasan, Gampong Pie, Indonesia. [4]Meteorological, Climatological, and Geophysical Agency, BMKG, Banda Aceh, Aceh, Indonesia.
- Email: *andreansimanjuntak@gmail.com*
- ORCID: 0000-0003-0623-0037
- Web of Science ResearcherID: NA
- Scopus Author ID: 57195483722
- Homepage: http://tdmrc.unsyiah.ac.id/

Bauer, K., Ph.D., Group Leader, Geophysical Imaging, Helmholtz Center Potsdam,German Research Center for Geosciences (GFZ), Albert-Einstein-Straße 42-46, Postdam, German.
- Email: *klaus.bauer@gfz-potsdam.de*
- ORCID: 0000-0002-7777-2653
- Web of Science ResearcherID: B-3325-2014
- Scopus Author ID: 0000-0002-7777-2653
- Homepage: https://www.gfz-potsdam.de/en/staff/klaus.bauer/sec22

Prof. Webber, M., Ph.D., Professor, Geophysical Imaging, Helmholtz Center Potsdam,German Research Center for Geosciences (GFZ), Albert-Einstein-Straße 42-46, Postdam, German.
- Email: *michael.weber@gfz-potsdam.de*
- ORCID: 0000-0002-3061-9758
- Web of Science ResearcherID: NA
- Scopus Author ID: 55468022900
- Homepage: https://www.gfz-potsdam.de/staff/michael.weber

HOW TO CITE THIS ARTICLE

Muksin, U.; Riana, E.; Rudyanto, A.; Bauer, K.; Simanjuntak, A.V.H.; Weber, M. (2023). Neural network-based classification of rock properties and seismic vulnerability. Global J. Environ. Sci.Manage., 9(1): 15-30.

DOI: https://dx.doi.org/10.22034/gjesm.2023.01.02

url: https://www.gjesm.net/article_252899.html